Electronic Supplementary Information

Hollow $Bi_4O_5Br_2$ Spheres Enable High-Density Bismuth Exposure for Enhanced Photocatalytic CO_2-to-CO conversion

Yong Li, Jingya Jiao, Han Zhang, Xingqun Li, Zhongqiu Wu, Quan Zhang, Hui Xu*

Y. Li, J. Jiao, H. Zhang, X. Li, Z. Wu, Prof. Q. Zhang, Prof. H. Xu

Institute for Energy Research, School of Agricultural Engineering, School of Environment and Safety Engineering

Jiangsu University, Zhenjiang, China

E-mail: quanzhang@ujs.edu.cn

Experimental section

2.1 Chemicals and materials

All chemicals and reagents were of analytical grade and required no further purification prior to use. $Bi(NO_3)_3 \cdot 5H_2O$ (AR), KBr (AR), ethanol, and ethylene glycol were purchased from Shanghai Sinopharm Group. All experiments employed deionized water with a resistivity of 18.2 MΩ cm^{-1}.

2.2 Synthesis

For hollow $Bi_4O_5Br_2$, typically, 3 mmol of $Bi(NO_3)_3$ $5H_2O$ was dissolved in 20 mL of ethyleneglycol, designated as Solution A; 2 mmol of KBr was dissolved in 60 mL of ethanol, designated as Solution B. Then, solution B was mixed with solution A and stirred uniformly for 0.5 h, simultaneously adjusting the pH to 10~11 using 1M NaOH solution. Subsequently, the prepared mixture was then transferred into a stainless steel autoclave lined with polytetrafluoroethylene and heated at 160 °C for 24 h. After reaction, the mixture was allowed to cool to room temperature. It was then washed three times with alternating deionized water and ethanol, followed by drying in a vacuum oven at 60 °C for 12 h to obtain the target sample.

The preparation of solid BiOBr followed the same procedure as for $Bi_4O_5Br_2$, except that 2 mmol of $Bi(NO_3)_3$ $5H_2O$ was used, and the solvothermal reaction time was set as 12 h.

2.3 Characterization

The crystal structures of the synthesized materials were analyzed by X-ray diffraction (XRD) on a Shimadzu XRD-6100 diffractometer equipped with a Cu Kα

source. Fourier transform infrared (FTIR) spectra were acquired on a Thermo Scientific Nicolet iS50 spectrometer over the range of 3000-500 cm^{-1}. SEM images and EDS maps were characterized using a JSM-7800F. TEM and HRTEM images were obtained using an electron microscope (Talos F200X G2) operated at 200 kV. Measure N_2 adsorption-desorption isotherms at 77 K using the Micromeritics Tristar II 3020 Surface Area and Pore Size Analyzer to obtain the Brunauer-Emmett-Teller (BET) surface area. X-ray photoelectron spectroscopy (XPS) was performed on a Thermo Scientific ESCALAB 250Xi. Optical absorption spectra were recorded in diffuse reflection mode using a UV-visible spectrophotometer (Rigaku UV-3600plus). The photoluminescence spectra (PL) was measured using a Cary Eclipse Spectrophotometer at an excitation wavelength of 360 nm, with a 75 W xenon lamp serving as the light source. The solid BiOBr and hollow $Bi_4O_5Br_2$ exhibit different geometric morphologies, in which the hollow spherical structure of $Bi_4O_5Br_2$ causes intense multiple scattering and diffuse reflection of incident excitation light and emitted photons, resulting in a certain difference in background signals compared to solid BiOBr.

The time-resolved photoluminescence (TRPL) curves were measured under 360 nm excitation recorded on a QM4m spectrometer. The CO_2 adsorption test was conducted using a fully automated Tristar II 3030 adsorption analyzer from Micromeritics. The degassing temperature was set to 100 °C, with an adsorption temperature of 25 ℃. Subsequently, CO_2 temperature-programmed desorption (CO_2-TPD) was tested using the TP-5080-B.

2.4 Photoelectrochemical measurement

Electrochemical characterization was performed with a CHI660B electrochemical workstation (Shanghai Chenhua) in a conventional three-electrode configuration. For photocurrent and electrochemical impedance spectroscopy (EIS) measurements, disperse 5 mg of catalyst in 1 mL of ethylene glycol and 5 μL of Nafion solution, then sonicate the mixture. Apply the mixture uniformly to the conductive surface of the FTO glass substrate and dry overnight in a 60 ℃ oven. Typically, FTO glass plates coated with catalyst samples serve as working electrodes, platinum wires function as counter electrodes, and silver chloride silver electrodes act as reference electrodes. A 0.2 M Na_2SO_4 solution is employed as the electrolyte, with a 300W xenon lamp providing illumination. Electrochemical impedance measurements were performed in KCl solution, with comparisons made between light (300 W Xenon lamp) and dark conditions. Under identical conditions, a 3-mm-diameter rotating disk electrode was used in place of the FTO glass electrode for LSV and CV testing, with 0.2 M Na_2SO_4 as the electrolyte. The working electrode was a Pt wire, and the reference electrode was Ag/AgCl electrode (filled with saturated KCl solution).

2.5 Photocatalytic performance evaluation

First, 10 mg of catalyst sample and disperse it in a 300-mL quartz reactor. Next, add a specific amount of sacrificial agent (composed of 4 mL triethanolamine and 12 mL ultrapure water). Ultrasonicate for 10 minutes to ensure complete dissolution of the catalyst in the sacrificial agent system. Evacuate the reactor containing the catalyst and purge with high-purity N_2 gas. Repeat this cycle three times to ensure stable reaction progression under a N_2 atmosphere. Maintain a pressure of approximately 85 kPa and

employ a 300 W xenon lamp as the light source. The reaction temperature was maintained at 10 °C by circulating cooling water through the outer wall, with the stirring speed set at 400 rpm. After 5 hours of irradiation, 1 mL of gas was withdrawn from the reactor. The gaseous products of CO, CH_4 and H_2 were detected and analyzed using a gas chromatograph (F60, Zhejiang Fuli Analytical Instrument Co., Ltd.) equipped with flame ionization detector (FID) and thermal conductivity detector (TCD).

2.6 *in-situ* FTIR test

Measure the *in-situ* FTIR spectrum of the sample using the Thermo Scientific Nicolet iS50. Place the sample uniformly on the substrate positioned at the center of the designed reaction cell. Purify with high-purity CO_2 (200 mL min^{-1}) for 20 minutes to remove physically adsorbed surface substances. Subsequently, high-purity CO_2 was continuously introduced into the test chamber at a flow rate of 200 mL min^{-1} via a custom-made bubbler until the feed gas adsorbed onto the catalyst surface and reached saturation. During measurement, the background was first collected under dark conditions. Subsequently, the lamp was kept illuminated, and signals were collected through the detector throughout the reaction process. Sample absorbance was measured every 6 minutes of irradiation.

2.7 *DFT calculations*

Density functional theory (DFT) calculations were performed using the Vienna Ab Initio Simulation Package (VASP).[S1] The electron-ion interaction was represented by the projector augmented wave (PAW), and the kinetic energy cutoff of plane wave was set as 400 eV. The PBE functional was utilized for geometry optimization.[S2-S3] The

gamma-centered (2 × 2 × 1) k-point mesh was utilized to calculate the electronic structure, and a vacuum slab with 15 Å thickness was applied. During optimization, the top two atomic layers were fully relaxed until the residual force was less than 0.02 $eV \cdot Å^{-1}$. The Gibbs free energy (ΔG) was evaluated by adding corrections from zero-point energy (ZPE) and vibrational entropy (S), which can be written as:

$$\Delta G = \Delta E_{DFT} + \Delta ZPE - T\Delta S$$

For the adsorbed species, ZPE and S were derived by frequency calculations with the harmonic oscillator approximation, and the VASPKIT code for post-processing of calculated data was adopted.[S4]

Figures

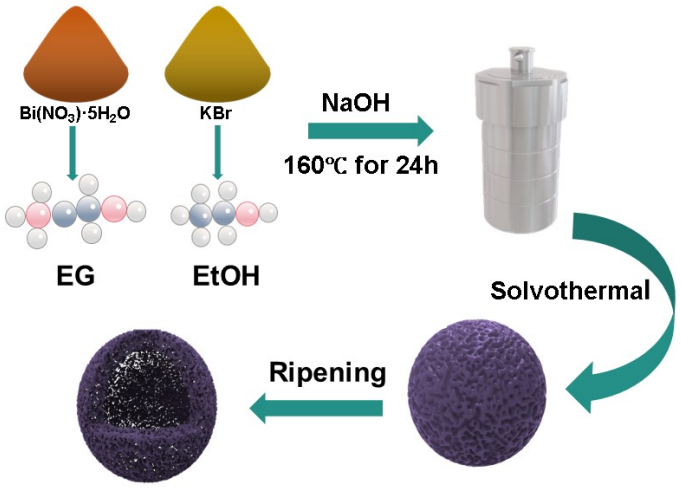

Fig. S1 Illustration of the formation of solid BiOBr and hollow $Bi_4O_5Br_2$ spheres.

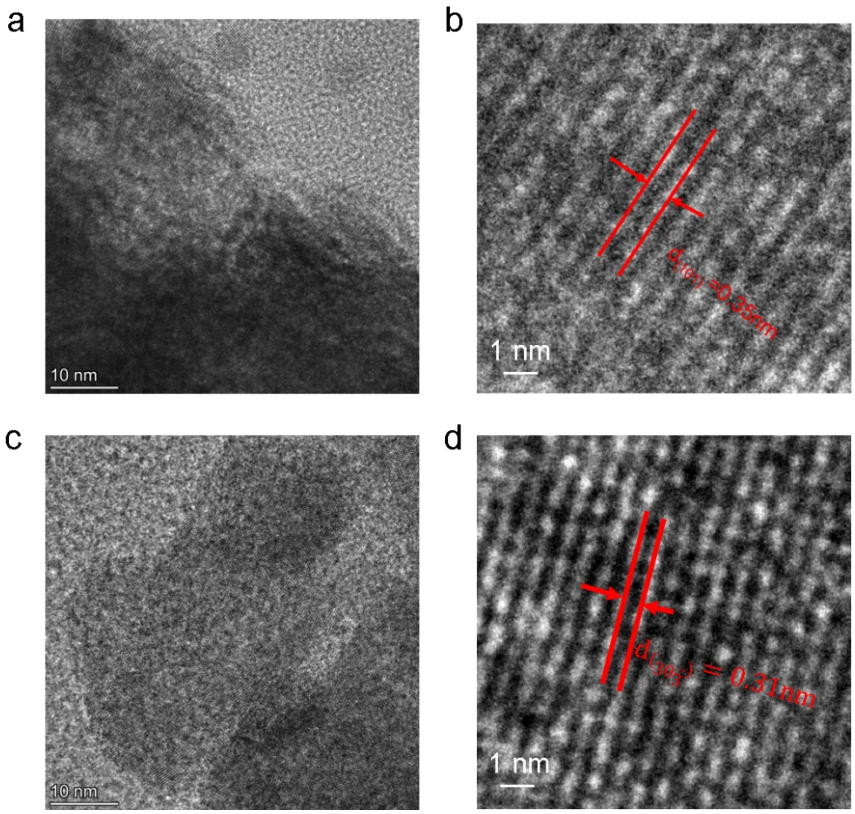

Fig. S2 HRTEM images of (a-b) solid BiOBr and (c-d) hollow $Bi_4O_5Br_2$ catalysts.

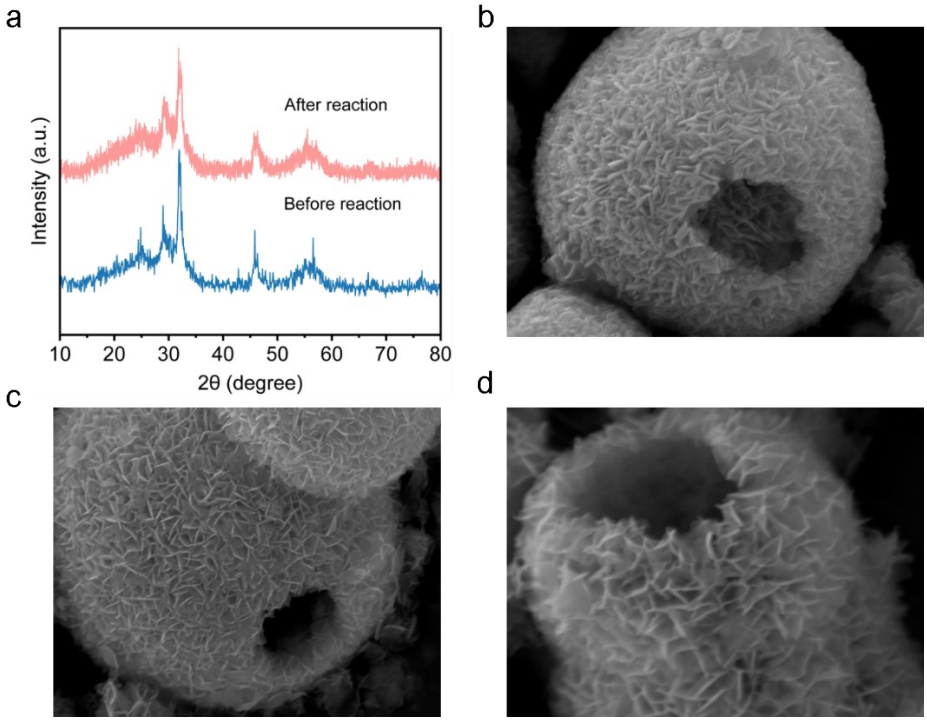

Fig. S3 (a) XRD patterns of $Bi_4O_5Br_2$ before and after reaction. (b) SEM image of fresh $Bi_4O_5Br_2$. (c-d) SEM images of used $Bi_4O_5Br_2$ after long-term reaction.

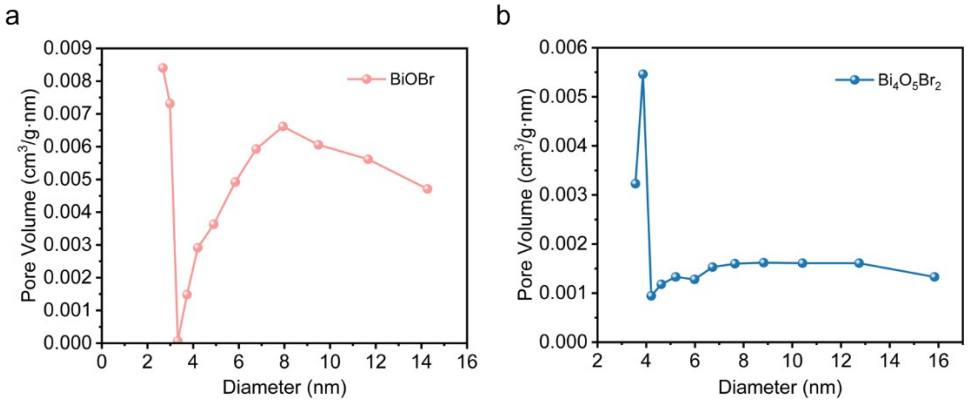

Fig. S4 Pore size distribution of (a) solid BiOBr and (b) hollow $Bi_4O_5Br_2$ catalysts.

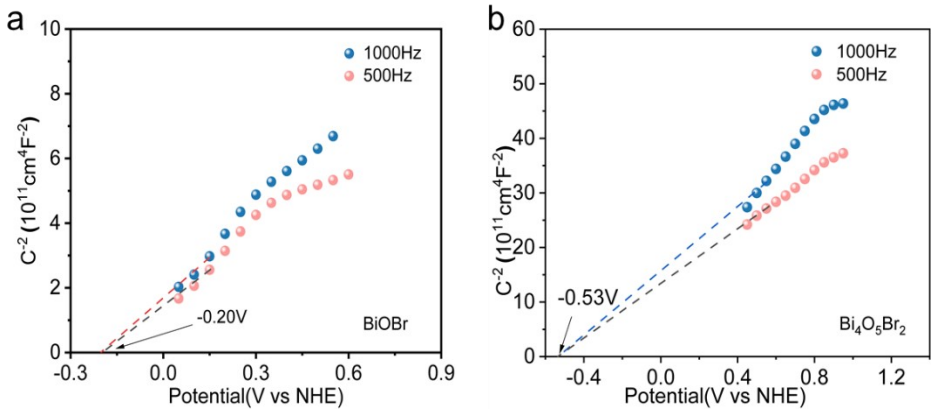

Fig. S5 Mott-Schottky plots of (a) solid BiOBr and (b) hollow $Bi_4O_5Br_2$ catalysts.

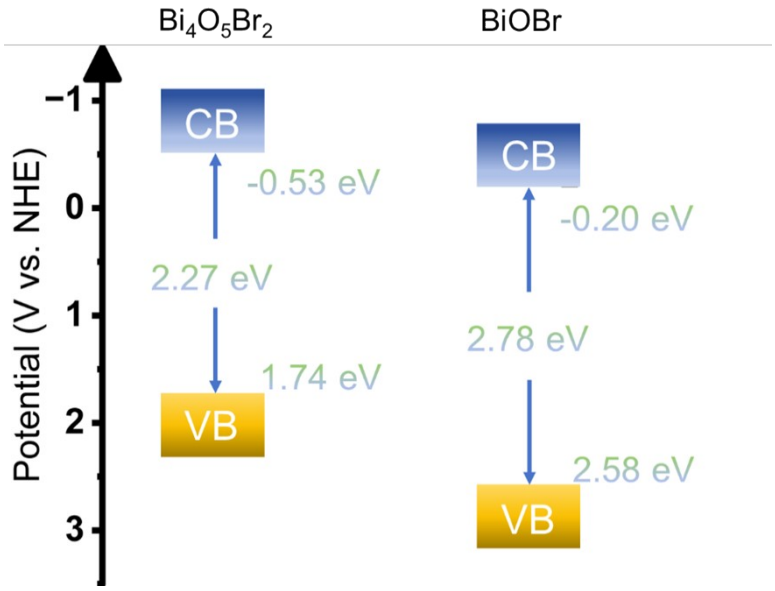

Fig. S6 Band alignment of solid BiOBr and hollow $Bi_4O_5Br_2$ catalysts.

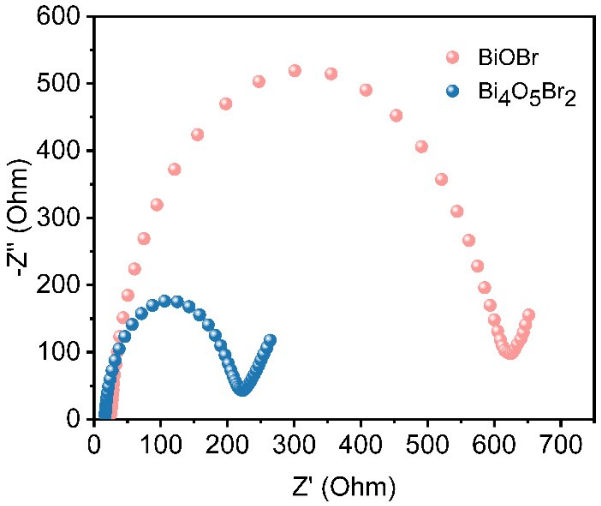

Fig. S7 Electrochemical impedance spectroscopy of solid BiOBr and hollow $Bi_4O_5Br_2$ under dark conditions.

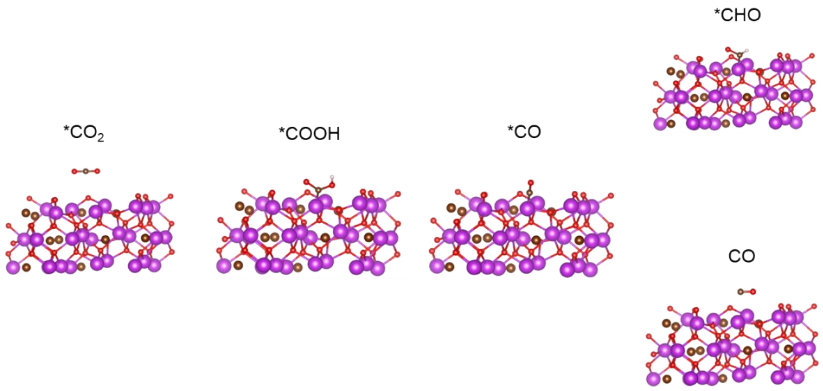

Fig. S8 The optimized $*CO_2$, *COOH, *CO, *CHO, and CO configurations on (002) surface of $Br_4O_5Br_2$ catalyst. The purple, brown, red, dark, and white spheres represent Bi, Br, O, C, and H atoms, respectively.

Table S1. Elemental Bi concentration (wt.%) determined by ICP-OES.

Samples	Element	Content C_0 (mg/L)	Percentage of Bi (wt.%)
BiOBr	Bi	10.6	63.8
$Bi_4O_5Br_2$	Bi	15.2	70.2

Table S2. Comparison of photocatalytic CO_2 reduction activity with reported Bi-based catalysts.

Catalysts	Light source	CO activity ($\mu mol\ g^{-1}\ h^{-1}$)	Reference
BiOBr/CoAl-LDH	300 W Xe lamp	4.096	S5
BiOI-D	300 W Xe lamp	3.02	S6
$SnO_2/Cs_3Bi_2Br_9$	300 W Xe lamp	0.28	S7
BiOBr-OVs	300 W Xe lamp	10.8	S8
Bi_2MoO_6/BiOI	300 W Xe lamp	8.34	S9
$BiOCl/In_2O_3$	300 W Xe lamp	6.9	S10
Hollow $Bi_4O_5Br_2$	**300 W Xe lamp**	**13.31**	**This work**

Reference

S1 G. Kresse, J. Furthmüller, *Phys. Rev. B,* 1996, **54**, 11169.

S2 V. Anisimov, J. Zaanen, O. Andersen, *Phys. Rev. B,* 1991, **44**, 943.

S3 J. Perdew, K. Burke, M. Ernzerhof, *Phys. Rev. lett.*, 1996, **77**, 3865.

S4 V. Wang, N. Xu, J.-C. Liu, G. Tang, W.-T. Geng, *Comput. Phys. Commun.*, 2021, **267**, 108033.

S5 Y. Lu, D. Wu, Y. Qin, Y. Xie, Y. Ling, H. Ye and Y. Zhang, *Sep. Purif. Technol.*, 2022, **302**, 122090.

S6 J. Xiong, X. Zhu, J. Xia and J. Di, *Appl. Surf. Sci.*, 2023, **627**, 157338.

S7 P. Hu, G. Liang, B. Zhu, W. Macyk, J. Yu and F. Xu, *ACS Catal.*, 2023, **13**, 12623-12633.

S8 J. Luo, X. Xue, W. Pan, T. Chen, Y. Jian, J. Zeng and W. Dong, *Appl. Catal. B*, 2025, **375**, 125442.

S9 Z. Wang, B. Cheng, L. Zhang, J. Yu, Y. Li, S. Wageh and A. A.Al-Ghamdi, *Chin. J. Catal.*, 2022, **43**, 1657-1666.

S10 X. Liu, H. Zhang, X. Qiu, H. Ye, Y. Xie and Y. Ling, *Appl. Catal. A*. 2024, **671**, 119574.